Phase-field model for epitaxial ferroelectric and magnetic nanocomposite thin films

J. X. Zhang,[a] Y. L. Li, D. G. Schlom, and L. Q. Chen
Department of Materials Science and Engineering, Pennsylvania State University, University Park, Pennsylvania 16802

F. Zavaliche and R. Ramesh
Department of Materials Science and Engineering and Department of Physics, University of California, Berkeley, California 94720

Q. X. Jia
MPA-STC, Los Alamos National Laboratory, Los Alamos, New Mexico 87545

(Received 21 September 2006; accepted 9 December 2006; published online 31 January 2007)

A phase-field model was developed for studying the magnetoelectric coupling effect in epitaxial ferroelectric and magnetic nanocomposite thin films. The model can simultaneously take into account the ferroelectric and magnetic domain structures, the electrostrictive and magnetostrictive effects, substrate constraint, as well as the long-range interactions such as magnetic, electric, and elastic interactions. As an example, the magnetic-field-induced electric polarization in $BaTiO_3-CoFe_2O_4$ nanocomposite film was analyzed. The effects of the film thickness, morphology of the nanocomposite, and substrate constraint on the degree of magnetoelectric coupling were discussed. © *2007 American Institute of Physics*. [DOI: 10.1063/1.2431574]

Magnetoelectric materials, which are simultaneously magnetic and ferroelectric, have drawn increasing interest due to their multifunctionality.[1,2] However, natural magnetoelectric single-phase crystals are rare and exhibit weak magnetoelectric coupling.[3] As a result, there have been many efforts to prepare synthetic magnetoelectrics, i.e., composites or solid solutions of ferroelectric and magnetic materials.[4–7] In addition to possessing the ferroelectricity and magnetism in each individual phase, composites are shown to exhibit an extrinsic magnetoelectric coupling. Recently, epitaxial $BaTiO_3-CoFe_2O_4$ (Ref. 8) and $BiFeO_3-CoFe_2O_4$ (Ref. 9) nanocomposite films have been deposited by using pulsed laser deposition, and magnetoelectric coupling phenomena have been observed directly. Calculations by Nan *et al.*[10] and Liu *et al.*[11,12] have shown that large magnetic-field-induced electric polarization (MIEP) could be produced in nanocomposite films due to the enhanced elastic coupling interaction.

The main purpose of this letter is to develop a phase-field model for predicting the magnetoelectric coupling effect for ferroelectric and magnetic nanocomposite thin films. The model simultaneously takes into account the ferroelectric and magnetic domain structures, the electrostrictive and magnetostrictive effects, substrate constraint, as well as the long-range interactions such as magnetic, electric, and elastic interactions. As an example, we will study the magnetoelectric response in the $BaTiO_3-CoFe_2O_4$ nanocomposite films, i.e., the magnetic-field-induced electric polarization. The effects of film thickness, morphology of nanocomposite, and substrate constraint on the magnetoelectric coupling will be investigated.

In the model, a given microstructure state is described by three fields: a local magnetization field $\mathbf{M}=M_s\mathbf{m}=M_s(m_1,m_2,m_3)$, a local polarization field $\mathbf{P}=(P_1,P_2,P_3)$, and an order parameter field η, which describes the spatial distributions of the two phases in the composite with $\eta=1$ for the magnetic phase and $\eta=0$ for the ferroelectric phase. M_s is the saturation magnetization. The total free energy of a ferroelectric/magnetic composite is, then, expressed by

$$F = F_{\text{anis}}(\mathbf{M}) + F_{\text{exch}}(\mathbf{M}) + F_{\text{ms}}(\mathbf{M}) + F_{\text{external}}(\mathbf{M},\mathbf{H}^e) + F_{\text{bulk}}(\mathbf{P}) + F_{\text{wall}}(\mathbf{P}) + F_{\text{elec}}(\mathbf{P}) + F_{\text{elas}}(\mathbf{P},\mathbf{M}), \quad (1)$$

where F_{anis}, F_{exch}, F_{ms}, F_{external}, F_{bulk}, F_{wall}, F_{elec}, and F_{elas} are the magnetocrystalline anisotropy energy, magnetic exchange energy, magnetostatic energy, external magnetic field energy, ferroelectric bulk free energy, ferroelectric domain wall energy, electrostatic energy, and elastic energy, respectively. $\mathbf{H}^e$ is the externally applied magnetic field.

The elastic energy can be calculated with

$$F_{\text{elas}}=\frac{1}{2}\int c_{ijkl}e_{ij}e_{kl}dV=\frac{1}{2}\int c_{ijkl}(\varepsilon_{ij}-\varepsilon^0_{ij})(\varepsilon_{kl}-\varepsilon^0_{kl})dV, \quad (2)$$

where e_{ij} is the elastic strain, ε_{ij} is the total strain, and c_{ijkl} is the elastic stiffness tensor. ε^0_{ij} is the stress-free strain due to the electostrictive effect or magnetostrictive effect, and is given by

$$\varepsilon^0_{ij}=\begin{cases}\eta\left[\frac{3}{2}\lambda_{100}\left(m_im_j-\frac{1}{3}\right)\right]+(1-\eta)(Q_{ijkl}P_kP_l) & (i=j),\\ \eta\left(\frac{3}{2}\lambda_{111}m_im_j\right)+(1-\eta)Q_{ijkl}P_kP_l & (i\neq j),\end{cases} \quad (3)$$

where Q_{ijkl} are the electrostrictive coefficients, and λ_{100} and λ_{111} are the magnetostrictive constants. The summation convention for the repeated indices is employed and $i, j, k, l=1, 2, 3$. The calculation of elastic energy for a film-substrate system[13] is obtained using a combination of Khachaturyan's mesoscopic elasticity theory[14] and Stroh's formalism of anisotropic elasticity.[15]

The mathematical expressions for the magnetocrystalline anisotropy energy, magnetic exchange energy, magnetostatic energy, external magnetic field energy, ferroelectric bulk free

[a]Electronic mail: jzz108@psu.edu

energy, ferroelectric domain wall energy, and electrostatic energy are exactly the same as those given in Refs. 16 and 17.

The temporal evolution of the magnetization configuration is described by the Landau-Lifshitz-Gilbert equation,

$$(1+\alpha^2)\frac{\partial \mathbf{M}}{\partial t} = -\gamma_0 \mathbf{M}\times\mathbf{H}_{\text{eff}} - \frac{\gamma_0\alpha}{M_s}\mathbf{M}\times(\mathbf{M}\times\mathbf{H}_{\text{eff}}), \quad (4)$$

where γ_0 is the gyromagnetic ratio, α is the damping constant, and $\mathbf{H}_{\text{eff}}$ is the effective magnetic field, which is given by $\mathbf{H}_{\text{eff}}=-(1/\mu_0 M_s)(\partial F/\partial \mathbf{m})$.

The temporal evolution of the polarization field is described by the time-dependent Ginzburg-Landau equation,

$$\frac{\partial P_i}{\partial t} = -L\frac{\delta F}{\delta P_i}, \quad (5)$$

where L is a kinetic coefficient related to the domain evolution.

We used a $BaTiO_3$–$CoFe_2O_4$ nanocomposite film as an example for our numerical simulations. The coefficients employed in the simulations are listed in Ref. 18.[19–23] The system was modeled by discretizing it into a three-dimensional array of cubic cells of $64\Delta x\times 64\Delta x\times 128\Delta x$, and periodic boundary conditions were applied along the x_1 and x_2 axes. The cell size in real space was chosen to be $\Delta x=l_0$, where $l_0=\sqrt{G_{110}/\alpha_0}$ and $\alpha_0=|\alpha_1|_{T=25\,^\circ\text{C}}$. We chose the gradient energy coefficient as $G_{11}/G_{110}=0.6$. If $l_0=1$ nm, $G_{110}=3.71\times10^{-11}$ $\text{C}^{-2}\,\text{m}^4\,\text{N}$, and the domain wall energy density is about 5×10^{-3} J m^{-2} for 180° domain wall, which is in line with existing experimental measurement and theoretical calculation.[24] In this work, we ignored the misfit strain along the ferroelectric-magnetic interface due to the lattice constant difference between the two phases for simplicity.

One measure of magnetoelectric response is the appearance of electric polarization upon applying an external magnetic field. The initial polarization of $BaTiO_3$ phase was chosen to be along the x_3 axis ($P_1=P_2=0$, $P_3>0$), which corresponds to the epitaxially grown single tetragonal c-phased $BaTiO_3$ under in-plane compressive substrate strain.[25] An external magnetic field $\mathbf{H}_e$ is applied, which is large enough to saturate the magnetic phase. By rotating the magnetic field from x_1 axis to x_3 axis, we simulated the evolution of the polarization in the ferroelectric phase, from which the MIEP, i.e., $\Delta\overline{P_3}=\overline{P_3}-\overline{P_3}(\mathbf{H}_e\|x_1)$, was calculated, where $\overline{P_3}$ is the effective (average) polarization of the entire composite film.

We started with 1-3 type $BaTiO_3$–$CoFe_2O_4$ nanocomposite film, with the $CoFe_2O_4$ pillars embedded in the $BaTiO_3$ matrix as shown in Fig. 1(a). The volume fraction of $CoFe_2O_4$ is chosen to be $f=0.35$ (similar to those studied in the experiments in Ref. 8), the thickness of the film is $h=16$ nm, and only one magnetic pillar was included in our model; therefore the distance between neighboring magnetic phases is $d=64$ nm and the radius of the pillar is $r=21.4$ nm. The constraint strains from the substrate were $\varepsilon_{11}^s=\varepsilon_{22}^s=-0.005$. The calculated effective (average) polarization of the composite was $\overline{P_3}(\mathbf{H}_e\|x_1)=0.180$ C m^{-2} when the applied magnetic field was along the x_1 axis, which is larger than that of a bulk single crystal sample (0.65×0.260 $\text{C m}^{-2}=0.169$ C m^{-2}) due to the compressive substrate strains. As shown in Fig. 1(b), with the rotation of the applied magnetic field, the effective (average) polarization of the composite increases gradually. To clarify the origin of MIEP, the stress distributions in the nanocomposite film were calculated. Since the film consists of single ferroelectric/magnetic domains, stress components σ_{11} and σ_{22} are almost constant along the film thickness direction. However, as can be seen in Fig. 2(a), component σ_{33} varies significantly with the film thickness, as it has to be zero at the film surface to satisfy the stress-free boundary condition. The change of the stress along the cross section at one-half of the film thickness with the applied magnetic field rotating from x_1 axis to x_3 axis is plotted in Figs. 2(b)–2(d). It is seen that the rotation of the applied magnetic field changes the stress distribution in the ferroelectric phase. As a result of the magnetostrictive effect, the magnetic phase deforms its shape with a change in magnetization. As λ_{100} is negative for $CoFe_2O_4$, the length of the magnetic phase increases along the x_1 axis and decreases along the x_3 axis after the rotation of the applied magnetic field, and consequently, the stress distribution in the neighboring ferroelectric phase changes through the elastic interaction between the two phases. Because of the piezoelectric effect, the change in stress distribution leads to a change in the polarization of the ferroelectric phase. For the electrostrictive constants we used, the decrease of σ_{11} (σ_{22}) ($\Delta\sigma_{11},\Delta\sigma_{22}<0$) in the ferroelectric phase increases the polarization along the x_3 axis (P_3), while the decrease of σ_{33}

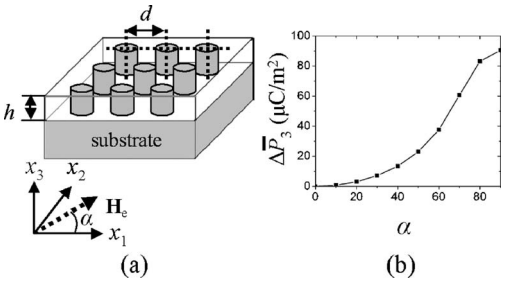

FIG. 1. (a) Schematic illustration of 1-3 type $BaTiO_3$–$CoFe_2O_4$ nanocomposite film with $CoFe_2O_4$ pillars (shaded) embedded in $BaTiO_3$ matrix (white). The applied magnetic field $\mathbf{H}_e$ is in the x_1-x_3 plane, and α is the angle between $\mathbf{H}_e$ and x_1 axis. (b) Dependence of the magnetic-field-induced electric polarization $\Delta\overline{P_3}=\overline{P_3}-\overline{P_3}(\mathbf{H}_e\|x_1)$ on the direction of the applied magnetic field ($f=0.35$, $h=16$ nm, $d=64$ nm, and $\varepsilon_{11}^s=\varepsilon_{22}^s=-0.005$).

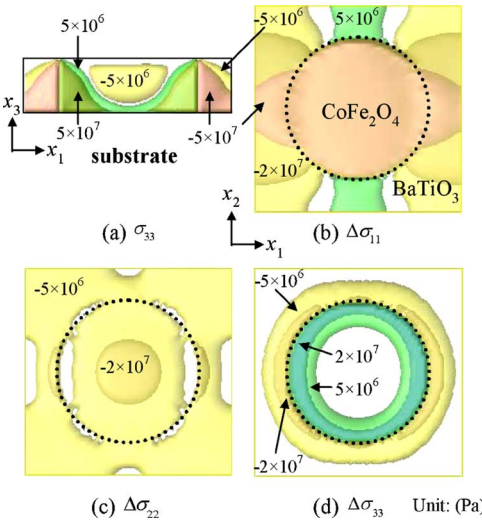

FIG. 2. (Color online) (a) Stress distribution (σ_{33}) when $\mathbf{H}_e\|x_1$ and [(b)–(d)] the change of stress distributions ($\Delta\sigma_{11}$, $\Delta\sigma_{22}$, and $\Delta\sigma_{33}$) when the applied magnetic field rotates from x_1 axis to x_3 axis [$\Delta\sigma_{ii}=\sigma_{ii}(\mathbf{H}_e\|x_3)-\sigma_{ii}(\mathbf{H}_e\|x_1)$, $f=0.35$, $h=16$ nm, $d=64$ nm, and $\varepsilon_{11}^s=\varepsilon_{22}^s=-0.005$].

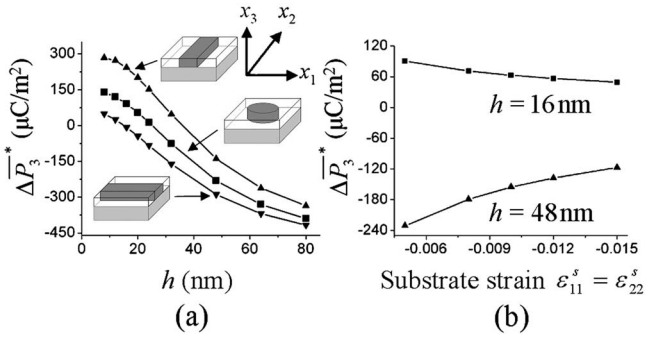

FIG. 3. (a) Dependence of magnetic-field-induced electric polarization $\Delta\overline{P_3}^* = \overline{P_3}(\mathbf{H}_e \| x_3) - \overline{P_3}(\mathbf{H}_e \| x_1)$ on the film thickness h ($f=0.35$ and $\varepsilon_{11}^s = \varepsilon_{22}^s = -0.005$). (b) Dependence of the magnetic-field-induced electric polarization $\Delta\overline{P_3}^*$ on the substrate strains ($f=0.35$ and $d=64$ nm).

($\Delta\sigma_{33} < 0$) reduces it. Therefore, $\Delta\overline{P_3}$ is determined by the competition of $\Delta\sigma_{11}$ ($\Delta\sigma_{22}$) and $\Delta\sigma_{33}$. In this example, $\Delta\sigma_{11}$ is dominant in enhancing the polarization of the nanocomposite film.

The dependence of MIEP on the film thickness was studied, and the results of $\Delta\overline{P_3}^* = \overline{P_3}(\mathbf{H}_e \| x_3) - \overline{P_3}(\mathbf{H}_e \| x_1)$ were presented in Fig. 3(a). With the increase of the film thickness, the effect of $\Delta\sigma_{33}$ becomes more important as the influence of the film surface is less significant. It was seen that the $\Delta\overline{P_3}^*$ decreases with the increase of the film thickness, and even becomes negative above a certain critical film thickness, since the decrease of σ_{33} ($\Delta\sigma_{33} < 0$) reduces $\overline{P_3}$ as we discussed above. Recent studies[26–28] have shown that different morphologies of epitaxial nanocomposite films could be obtained by controlling the volume fractions of the phases or the substrate's thickness and orientation. Therefore, we studied as well the MIEP for two stripelike nanocomposites as shown in the inset of Fig. 3(a). (The volume fraction of $CoFe_2O_4$ was fixed to be $f=0.35$.) From Fig. 2(b) we can see that the change of σ_{11} is mostly along the sides of the magnetic phase in the x_1 direction. The stripelike morphologies could enhance or decrease the effect of $\Delta\sigma_{11}$ depending on the orientation of its periodic distribution. As shown in Fig. 3(a), compared to the 1-3 type nanocomposite with magnetic pillars in a ferroelectric matrix, $\Delta\overline{P_3}^*$ becomes larger for the stripelike morphology that distributes periodically along the x_1 axis, while $\Delta\overline{P_3}^*$ is smaller for the stripelike morphology that distributes periodically along the x_2 axis. The difference is more significant for thin films for which the effect of $\Delta\sigma_{11}$ dominates.

It is expected that the constraint of the substrate will also play an important role in the MIEP since it can affect the stress distribution in the film dramatically. Figure 3(b) shows $\Delta\overline{P_3}^*$ obtained under various compressive substrate strains for 1-3 type nanocomposite films with two different thicknesses. With the increase of the magnitude of compressive substrate strains, the magnitude of $\Delta\overline{P_3}^*$ decreases for both films. This indicates that under a large substrate compressive strain, it becomes difficult to change the polarization of the ferroelectric phase through elastic coupling.

It should be emphasized that the phase-field approach presented here is three-dimensional and considers the microstructure of the nanocomposite that is proved to be critical to the magnetoelectric coupling in the nanocomposite. The elastic energy in the constrained thin film was incorporated, including the effect of free film surface and the constraint from the substrate. All prior studies essentially considered two-dimensional structures and the effect of thin film boundary condition was included only approximately.

In summary, we have developed a phase-field model to predict the magnetoelectric coupling in a nanocomposite thin film made up of ferroelectric and magnetic materials. The magnetic-field-induced electric polarization (MIEP) in $BaTiO_3$–$CoFe_2O_4$ nanocomposite films was analyzed. The simulation showed that the MIEP is highly dependent on the film thickness, morphology of the nanocomposite, and substrate constraint, which provide a number of degrees of freedom in controlling coupling in nanocomposite films.

The authors are grateful for the financial support of the National Science Foundation under Grant Nos. DMR-0507146 and DMR 01-22638, Penn State MRI seed grant, and Laboratory-Directed Research and Development at Los Alamos National Laboratory. One of the authors (L.Q.C.) would also like to acknowledge the support from the Guggenheim Foundation through a fellowship.

[1] M. Fiebig, J. Phys. D **38**, R123 (2005).
[2] N. A. Spaldin and M. Fiebig, Science **309**, 391 (2005).
[3] W. Prellier, M. P. Singh, and P. Murugavel, J. Phys.: Condens. Matter **17**, R803 (2005).
[4] G. Harshe, Ph.D. thesis, Pennsylvania State University, 1991.
[5] S. X. Dong, J. R. Cheng, J. F. Li, and D. Viehland, Appl. Phys. Lett. **83**, 4812 (2003).
[6] J. Ryu, S. Priya, K. Uchino, and H. Kim, J. Electroceram. **8**, 107 (2002).
[7] J. Zhai, N. Cai, Z. Shi, Y. Lin, and C. W. Nan, J. Appl. Phys. **95**, 5685 (2004).
[8] H. Zheng, J. Wang, S. E. Lofland, Z. Ma, L. Mohaddes-Ardabili, T. Zhao, L. Salamanca-Riba, S. R. Shinde, S. B. Ogale, F. Bai, D. Viehland, Y. Jia, D. G. Schlom, M. Wuttig, A. Roytburd, and R. Ramesh, Science **303**, 661 (2004).
[9] F. Zavaliche, H. Zheng, L. Mohaddes-Ardabili, S. Y. Yang, Q. Zhan, P. Shafer, E. Reilly, R. Chopdekar, Y. Jia, P. Wright, D. G. Schlom, Y. Suzuki, and R. Ramesh, Nano Lett. **5**, 1793 (2005).
[10] C. W. Nan, G. Liu, Y. Lin, and H. Chen, Phys. Rev. Lett. **94**, 197203 (2005).
[11] G. Liu, C. W. Nan, Z. K. Xu, and H. Chen, J. Phys. D **38**, 2321 (2005).
[12] G. Liu, C. W. Nan, and J. Sun, Acta Mater. **54**, 917 (2006).
[13] Y. L. Li, S. Y. Hu, Z. K. Liu, and L. Q. Chen, Acta Mater. **50**, 395 (2002).
[14] A. G. Khachaturyan, *Theory of Structural Transformation in Solids* (Wiley, New York, 1983), p. 198.
[15] A. N. Stroh, J. Math. Phys. **41**, 77 (1962).
[16] J. X. Zhang and L. Q. Chen, Acta Mater. **53**, 2845 (2005).
[17] Y. L. Li and L. Q. Chen, Appl. Phys. Lett. **88**, 072905 (2006).
[18] For $BaTiO_3$, $\alpha_1 = 4.124(T-115)\times 10^5$, $\alpha_{11} = -2.097\times 10^8$, $\alpha_{12} = 7.974\times 10^8$, $\alpha_{111} = 1.294\times 10^9$, $\alpha_{112} = -1.950\times 10^9$, $\alpha_{123} = -2.500\times 10^9$, $\alpha_{1111} = 3.863\times 10^{10}$, $\alpha_{1112} = 2.529\times 10^{10}$, $\alpha_{1122} = 1.637\times 10^{10}$, $\alpha_{1123} = 1.367\times 10^{10}$, $Q_{11} = 0.10$, $Q_{12} = -0.034$, and $Q_{44} = 0.029$. For $CoFe_2O_4$, $M_s = 4\times 10^5$, $\lambda_{100} = -590\times 10^{-6}$, $\lambda_{111} = 120\times 10^{-6}$, $K_1 = 3\times 10^5$, $K_2 = 0$, and $A = 7\times 10^{-12}$. $T = 25$ °C. For simplicity, we assumed elastic homogeneity in this work, and the elastic constants of $BaTiO_3$ are used, i.e., $c_{11} = 1.78\times 10^{11}$, $c_{12} = 0.96\times 10^{11}$, and $c_{44} = 1.22\times 10^{11}$ (in SI units).
[19] Y. L. Li, L. E. Cross, and L. Q. Chen, J. Appl. Phys. **98**, 064101 (2005).
[20] T. Yamada, J. Appl. Phys. **43**, 328 (1972).
[21] Y. Suzuki, R. B. van Dover, E. M. Gyorgy, J. M. Phillips, and R. J. Felder, Phys. Rev. B **53**, 14016 (1996).
[22] R. M. Bozorth, E. F. Tilden, and A. J. Williams, Phys. Rev. **99**, 1788 (1955).
[23] A. F. Devonshire, Philos. Mag. **42**, 1065 (1951).
[24] J. Padilla, W. Zhong, and D. Vanderbilt, Phys. Rev. B **53**, R5969 (1996).
[25] K. J. Choi, M. Biegalski, Y. L. Li, A. Sharan, J. Schubert, R. Uecker, P. Reiche, Y. B. Chen, X. Q. Pan, V. Gopalan, L. Q. Chen, D. G. Schlom, and C. B. Eom, Science **306**, 1005 (2004).
[26] H. M. Zheng, Q. Zhan, F. Zavaliche, M. Sherburne, F. Straub, M. P. Cruz, L. Q. Chen, U. Dahmen, and R. Ramesh, Nano Lett. **6**, 1401 (2006).
[27] A. Artemev, J. Slutsker, and A. L. Roytburd, Acta Mater. **53**, 3425 (2005).
[28] J. Slutsker, I. Levin, J. H. Li, A. Artemev, and A. L. Roytburd, Phys. Rev. B **73**, 184127 (2006).